

# Non-parabolicity, band gap re-normalisation and carrier scattering in Si doped ZnO

R. E. Treharne<sup>a,\*</sup>, L. J. Phillips<sup>a</sup>, K. Durose<sup>a</sup>, A. D. Weerakkody<sup>b</sup>, I. Z. Mitrovic<sup>b</sup>, S. Hall<sup>b</sup>

<sup>a</sup>*Stephenson Institute for Renewable Energy, University of Liverpool, UK*

<sup>b</sup>*Department of Electrical Eng. and Electronics, University of Liverpool, UK*

---

## Abstract

*Keywords:* zinc oxide, magnetron sputtering, thin-film, doping, non-parabolicity, band gap normalisation

---

## 1. Introduction

Polycrystalline ZnO films have received significant attention in recent years. They can be degenerately doped by incorporating group III (e.g. Al, Ga or In [1]) or group VII (e.g. F [2, 3], Cl [4]) elements to achieve resistivities of the order  $10^{-4} \Omega\cdot\text{cm}$  while maintaining a high optical transparency,  $> 90\%$ . Such ZnO based transparent conducting oxide (TCO) films, most notably Al doped ZnO (AZO), are now used extensively within thin-film photovoltaic technologies (namely CIGS, CZTS and CdTe) and have widely replaced the use of indium based TCOs. A wide range of deposition techniques have been demonstrated for ZnO films including atomic layer deposition (ALD) [5], metal-organic chemical vapour deposition (MOCVD) [6], pulsed laser deposition (PLD) [7] and magnetron sputtering [1, 8, 9].

They key property of a TCO is its resistivity, which in the context of thin-film PV, should be as low as possible. Film transmittance will generally remain high over the visible wavelength range for a wide range of resistivities, except in

---

\*Corresponding author

Email address: R.Treharne@liverpool.ac.uk (R. E. Treharne)

the case of exceptionally high free carrier concentrations (i.e.  $> 10^{21} \text{ cm}^{-2}$ ), and so is of secondary concern experimentally. The most common approach to minimising a TCO's resistivity, with respect to any experimental parameter (e.g. pressure, temperature, composition), is to generate large sample sets over which a single experimental parameter is varied incrementally. Such investigations are time consuming and the experimental consistency from sample to sample can be poor due to uncontrollable drifts in other deposition parameters. Furthermore, even for large sample sets the relationship determined between the resultant film properties and the deposition conditions can often be ambiguous. This is particularly true for resistivity which is highly sensitive and can vary on the scale of several orders of magnitude for a very narrow range of composition.

In this work, a combinatorial methodology is developed for the study of TCO materials, in this case Si doped ZnO (SZO). The approach eliminates the need for large sample sets and generates results that are highly consistent and reliable. We demonstrate how the methodology can be used to investigate fundamental properties of the material, namely conduction band non-parabolicity and band gap re-normalization, as well as more empirical relationships such as the compositional dependence of electrical properties. Furthermore, the consideration of a grain boundary limited scattering mechanism to describe the observed behaviour in SZO leads to the proposal of an extension to the current theory to apply in the case of degenerately doped polycrystalline films.

## 2. Experimental Methods

Films were deposited via RF magnetron sputtering using an AJA Phase II-J Orion system. The system was configured in a 'sputter-up' geometry with the substrate being suspended above two separate ceramic targets of ZnO and  $\text{SiO}_2$  arranged off-centre and tilted at  $5^\circ$  towards the centre of the substrate. Soda-lime glass substrates (OptiWhite<sup>TM</sup>, NSG Pilkington) of size  $100 \times 100 \times 4 \text{ mm}^3$  were cleaned by scrubbing with a nylon brush and a series of de-ionized water and isopropanol alcohol rinses followed by blow drying with a nitrogen gas jet.

During deposition the ZnO and SiO<sub>2</sub> targets were sputtered from simultaneously using powers of 150 W and 50 W respectively. A growth pressure of  $2.7 \times 10^{-3}$  mbar Ar was used during deposition. The substrate temperature was maintained at  $350 \pm 5^\circ\text{C}$  during growth and the substrate was kept static with respect to the magnetrons (i.e the substrate was not rotated). Deliberate gradients of both thickness and composition were subsequently achieved across the resultant film to generate a ‘combinatorial’ sample. A second film of pure SiO<sub>2</sub> was deposited under identical conditions (but without ZnO) to generate a reference film for estimating the % wt. profile of SiO<sub>2</sub> in the co-sputtered combinatorial sample.

A Shimadzu UV-Vis-IR 3700 spectrophotometer with mapping capability was used to measure the transmittance of the co-sputtered film over the range 250 - 2500 nm. 289 spectra were taken in total at 5 mm increments over the full sample surface. At each of these 289 points the sheet resistance was also measured using a CMT-SR2000 4-point probe mapping system. Following transmittance and sheet resistance measurements the sample was cut into one hundred  $10 \times 10 \text{ mm}^2$  pieces. A selection of these pieces, 10 in total, were further scribed into four  $5 \times 5 \text{ mm}^2$  sections and Hall measurement were performed on each of these sections. Hall measurements were performed with custom built equipment, provided by Semimetrix Ltd., using a field strength of 0.8 T. Ellipsometry was performed on the same sections using a Woollam M2000-UI system. Ellipsometry was also used to map the thickness profile of the pure SiO<sub>2</sub> reference film.


### 3. Results

#### 3.1. Fitting of optical spectra

Figure 1 shows a typical transmittance spectra taken from a single point on the combinatorial ZnO:Si sample and the corresponding fit achieved using a theoretical model of the material’s dielectric permittivity  $\varepsilon(\omega)$ . Full details of this model are given in [10]. The key components of the model include: 1) a Lorentzian oscillator to account for the behaviour of the system’s bound


74 electrons and to provide a smoothly varying dielectric background over the range  
 75 of interest (250–2500 nm), 2) an extended Drude model [11], to characterise the  
 76 system’s free electron response, and 3) an inter-band transition model to account  
 77 for the steep increase in the material’s absorption coefficient ( $\alpha \propto (E - E_G)^{1/2}$ )  
 78 in the vicinity of its direct band gap (3.3 – 3.4 eV). The two key parameters  
 79 extractable from the dielectric model are the film’s thickness,  $d$ , and plasma  
 80 frequency,  $\omega_p$ , which is related directly to the carrier concentration according  
 81 to

$$\omega_p = \sqrt{\frac{n_e e^2}{m_e \varepsilon_\infty \varepsilon_0}} \quad (1)$$

82 where  $m_e$  is the effective electrons (expressed in units of the free electron mass,  
 83  $m_0$ ),  $\varepsilon_\infty$  is the material’s high frequency relativity permittivity ( $\sim 8.3$  for single  
 84 crystal ZnO [12]) and  $\varepsilon_0$  is the permittivity of free space.  optical dispersion  
 85 for the material, i.e. refractive index  $n$  and extinction coefficient  $\kappa$  are also  
 86 extracted from the fitting procedure and are shown in the inset of figure 1.

87 Fitting was achieved by using a Nelder-Mead downhill simplex algorithm  
 88 [13], implemented via python script, to minimize the quantity

$$\chi^2 = \sum_i^N \sqrt{\frac{y_i - O_i}{N^2}} \quad (2)$$

89 where  $N$  is the total number of data points in the spectra,  $O_i$  the observed  
 90 transmittance at each wavelength over the range of interest, and  $y_i$  the the-  
 91 oretical transmittance calculated using the transfer matrix method [14] for a  
 92 single thin-film on a finite, transparent substrate. The fitting algorithm was it-  
 93 erated until the relative fractional change in consecutive  $\chi^2$  values was less than  
 94  $1 \times 10^{-6}$ . The fitting of all 289 transmittance spectra taken over the combina-  
 95 torial sample was fully automated, the only user input required being an initial  
 96 estimate of film thickness at the point of the first spectrum. This automation  
 97 ensured that the fitting of consecutive spectra was highly consistent. For all  
 98 spectra,  $\chi^2$  values of  $< 1$   e achieved indicating that all fits were as successful  
 99 as that shown in figure 1.

100 It was not possible to extract values for the true optical band-gap  $E_G$  from

the inter-band transition component of the mode [1] all values were typically  
 $\sim 0.2$  eV lower than expected (even once non-parabolicity and re-normalisation  
effects had been accounted for, see sections 3.2 and 4). This is due to the pres-  
ence of a population of impurity states located in energy just below the bottom  
of the conduction band. The presence of these states generate a broadening,  
commonly referred to as an ‘Urbach tail’ [1] in the onset of the absorption  
coefficient. It is very difficult to determine the extent of this broadening by fit-  
ting the dielectric model to a single transmittance spectra. The use of variable  
angle spectroscopic ellipsometry (VASE) permitted the determination of the true  
band gap of the material as it only probed the interface of the films and did not  
sample the Urbach states.

For each point over the combinatorial sample ellipsometric spectra were  
taken at angles of  $65^\circ$  and  $70^\circ$  with respect to a plane normal to the sample  
surface. The spectra were and fitted using a parameterized semi-conductor  
(PSEMI-M0) model [16] over the range  $350 - 1000$  nm. Figure 2 shows a typical  
fit achieved by the model and the inset shows the difference in the  $\alpha^2$  versus  
 $E$  behaviour extracted from transmittance and ellipsometry data respectively.  
This disparity between band gaps extracted from the two techniques is in good  
agreement with that reported previously by Srikant [17] in ZnO.

### 3.2. Conduction band non-parabolicity

For highly doped metal-oxides it has been shown that the conduction band,  
 $E_c$ , is ‘non-parabolic’ and that the origin of this non-parabolicity may be at-  
tributed to a carrier dependent effective mass,  $m_e(n_e)$ . The functional form of  
this dependence, first suggested by Pisarkiewicz *et. al* [18], is given by

$$m_e(n_e) = m_{e0} \sqrt{1 + \frac{2C\hbar^2 k}{m_{e0}}} \quad (3)$$

where  $m_{e0}$  is the value of the effective mass at the conduction band minimum  
and  $C$  is the non-parabolicity factor, expressed in  $\text{eV}^{-1}$ . The carrier wave-  
number can be expressed in terms of the carrier concentration according to  $k =$   
 $(3\pi^2 n_e)^{1/3}$ . By re-examining equation 1 it is clear that the relationship between

129  $\omega_p^2$  and  $n_e$  is becomes non-linear if the effective mass is not a constant. Figure 3  
 130 shows a plot of  $\omega_p$ , extracted from the spectrophotometry measurements, versus  
 131 the carrier concentration,  $n_e^H$ , determined via Hall measurements, for the sample  
 132 subset cut from the original combinatorial sample. A similar  $\chi^2$  minimization  
 133 procedure to that described in section 3.1, in which the fitting parameters were  
 134  $m_{e0}$  and  $C$ , was applied to the data set using

$$\chi^2 = \sum_{i=1}^n \frac{(n_{e_i}^S - n_{e_i}^H)^2}{n^2} \quad (4)$$

135 where the superscript  $S$  corresponds to carrier concentrations calculated, us-  
 136 ing a carrier dependent effective mass  $m_e(n_e)$  (equations (1) a 3), from the  
 137 spectroscopically determined plasma frequencies. The superscript  $H$  denotes  
 138 values of  $n_e$  determined directly via Hall measurements. To determine the un-  
 139 certainty associated with the fitted  $m_{e0}$  and  $C$  values a Monte-Carlo style error  
 140 treatment [19] was implemented within which the  $\chi^2$  minimization procedure  
 141 was performed 1000 times. The inset plot in figure 3 shows the mean  $m_e(n_e)$   
 142 relationship (solid line) and the corresponding spread (yellow line). An average  
 143 extracted value of  $m_{e0} = 0.35 \pm 0.02 m_0$  is higher than previous published values  
 144 of  $0.24 - 0.28 m_0$  for the effective mass in undoped ZnO. An average extracted  
 145 value of  $C = 0.30 \pm 0.01$  eV agrees very well with previously reported values of  
 146  $\sim 0.29$  eV<sup>-1</sup> [9, 20] for Al doped ZnO films.

### 147 3.3. Band-gap renormalization

148 The optical band gap of a degenerately doped metal-oxide system increases  
 149 as a function of carrier concentration (Burstein-Moss shift [21, 22] according to

$$E_G = E_{G0} + \frac{\hbar^2(3\pi^2 n_e)^{2/3}}{2m_{eff}} \quad (5)$$

150 where  $E_{G0}$  is the band-gap at the conduction band minimum and the joint den-  
 151 sity of states effective mass,  $m_e$ , given as

$$\frac{1}{m_{eff}} = \frac{1}{m_h} + \frac{1}{m_e(n_e)} \quad (6)$$

152 A constant hole effective mass value of  $m_h = 0.7m_0$  [ ] assumed throughout  
 153 this work. Note that the non-parabolicity of the conduction band is accounted  
 154 for when estimating the band gap by using the carrier dependent effective mass  
 155  $m_e(n_e)$  determined in section 3.2. The data points in figure 4 show the band-  
 156 gap values, determined via ellipsometry, plotted against the Hall carrier con-  
 157 centrations. The points lie some distance from the relationship predicted by  
 158 equation 5. The apparent reduction in the real band-gap values is due the re-  
 159 normalization effects of many body electron-electron, electron-ion and hole [ ]  
 160 interactions. Lu *et. al* [23] have shown that the total energy shift due to re-  
 161 normalization can be estimated by parameterising the detailed model described  
 162 by Jain *et. al* [24, 25] according to

$$E_R = An_e^{1/3} + Bn_e^{1/4} + Cn_e^{1/2} \quad (7)$$

163 where  $E_R$  is negative with respect to  $E_G$ . The  $n_e^{1/3}$ ,  $n_e^{1/4}$  and  $n_e^{1/2}$  dependencies  
 164 correspond to the exchange energy of free electrons, their correlation energy  
 165 and the electron-ion interaction energy respectively. The coefficients  $A$ ,  $B$ , and  
 166  $C$ , quantify the strength of each of these three dependencies. The coefficient  
 167 values for the data shown in figure 4, and a value for  $E_{G0}$ , was extracted using  
 168 the established minimisation procedure. Table 1 sh [ ] the extracted values  
 169 and comparative values for n-type ZnO thin-films. The strength of the  $n_e^{1/3}$   
 170 dependence is roughly three times than that reported for Al doped ZnO. [ ]

#### 171 4. Mapping of compositional dependence

172 Film thickness profiles were determined for the combinatorial ZnO:Si and  
 173 SiO<sub>2</sub> samples. The % wt. SiO<sub>2</sub> content at each point over the combinatorial  
 174 sample was estimated according to

$$x = \frac{\Gamma_B d_B}{\Gamma_A d_A + \Gamma_B d_B} \times 100\% \quad (8)$$

175 where  $\Gamma_A$  and  $\Gamma_B$  are the bulk densities of ZnO and SiO<sub>2</sub> respectively and  $d_A$  and  
 176  $d_B$  are the corresponding thicknesses,  $d$ , of the ZnO and SiO<sub>2</sub> films. The carrier

177 concentration profile for the combinatorial sample was calculated from extracted  
 178  $\mu_e$  values according to equation 1 and using the non-parabolic effective mass  
 179 relationship,  $m_e(n_e)$ , determined in section 3.2. The corresponding mobility  
 180 profile was calculated according to

$$\mu_e = \frac{1}{n_e^S R_S de} \quad (9)$$

181 where  $R_S$  are the sheet resistance values obtained directly from 4 point probe  
 182 measurements. Figure 5 shows the three dimensional contour profiles of  $n_e$  and  
 183  $\mu_e$  accross the surface of the combinatorial sample. In both cases, a maximal  
 184 ridge, corresponding to  $n_e \sim 4.5 \times 10^{18} \text{ cm}^{-3}$  and  $\mu_e \sim 16 \text{ cm}^2 \text{ V}^{-1} \text{ s}^{-1}$ , runs diagonally  
 185 across the sample. By superimposing the contour distribution of % wt.  $\text{SiO}_2$   
 186 content (dotted black contour lines) a very strong correlation between carrier  
 187 concentration and composition becomes apparent, the maximum  $n_e$  and  $\mu_e$   
 188 values corresponding to a value of  $x = 0.65\%$  wt.  $\text{SiO}_2$  content.

189 By plotting the distributions of  $n_e$  and  $\mu_e$  with respect to  $x$  the compositional  
 190 dependence can be observed directly, see figure 6. Here the strength of the  
 191 combinatorial analysis is fully appreciated by its ability to generate continuous,  
 192 non-ambiguous distributions of the material's electrical behaviour and shows  
 193 that it is highly sensitive to the composition - the resistivity spanning over three  
 194 orders of magnitude within the compositional range  $x = 0 - 0.65\%$  wt.  $\text{SiO}_2$ .  
 195 Furthermore, the uncertainty in the optimum value of  $x$ , that minimises the  
 196 resistivity, is significantly reduced when compared to the multi-sample analyses  
 197 that are commonly reported.

198 The solid straight line in the  $n_e$  vs  $x$  plot indicates the relationship predicted  
 199 for a 100% doping efficiency, i.e. where every Si atom incorporated into film  
 200 substitutionally replaces a Zn atom and contributes two free electrons to the sys-  
 201 tem. For low values of  $x$ , i.e. in the range  $0 - 0.65\%$  wt.  $\text{SiO}_2$ , this relationship  
 202 is adhered to. However as  $x$  increases further the doping efficiency decreases  
 203 rapidly and the carrier concentration is limited to  $3 - 4 \times 10^{18} \text{ cm}^{-3}$  for composi-  
 204 tions up to  $10\%$  wt.  $\text{SiO}_2$ . After the optimum value of  $x$  is reached the mobility  
 205 drops off steeply and approaches a value of zero for values of  $x$  beyond  $6\%$ .



206 This suggests that as  $x$  is increased beyond the optimum composition, Si is no  
 207 longer incorporated into the film as a substitutional dopant and instead acts to  
 208 increase the scattering of the free carriers, existing as an interstitial impurities  
 209 or forming segregated Si-O phases at the grain boundaries.

#### 210 4.1. Scattering

211 The behaviour of carrier mobility can be described further by considering  
 212 its direct relationship with the carrier concentration. Figure 5 shows that by  
 213 plotting  $\mu_e$  versus  $n_e$  for all data points two distinct populations are revealed.  
 214 The red data points correspond to compositions  $x < 0.65\%$ . Within this distri-  
 215 bution, and for carrier concentrations below  $2.5 \times 10^{18} \text{ cm}^{-3}$  the mobility of the  
 216 free carriers can be described in terms of a grain barrier limited transport model  
 217 proposed by Seto *et.al* [26]. The model assumes that at the grain boundaries  
 218 a population of filled trap states exist within the band gap. This causes the  
 219 conduction band to bend upwards at each grain boundary forming a barrier  
 220 to charge transport. The inter-grain mobility,  $\mu_B$  of free carriers is therefore  
 221 limited by thermal processes according to

$$\mu_{ig} = \mu_0 \exp\left(-\frac{\Phi_B}{k_B T}\right) \quad (10)$$

222 where  $\Phi_B$  is the barrier height at the grain boundary and is related directly to  
 223 the carrier concentration according to

$$\Phi_B = \frac{e^2 n_t}{8 \varepsilon_\infty \varepsilon_0 n_e} \quad (11)$$

224 where  $n_t$  is the trap density and  $\varepsilon_\infty$  is the high frequency dielectric permittivity  
 225 ( $\varepsilon_\infty \sim 8.3$  for single crystal ZnO [12]). The pre-factor  $\mu_0$  is the internal mobility  
 226 of the grain, expressed as

$$\mu_0 = \frac{eL}{\sqrt{2\pi m_e k_B T}} \quad (12)$$

227 where  $L$  is the grain size. It is necessary to extend the Seto model in the case  
 228 of degenerately doped ZnO to account for the tunnelling of carriers through the  
 229 barrier  $\Phi_B$ . As the carrier concentration increases the Fermi level rises towards  
 230 the top of the barrier while the barrier height decreases proportionally to  $1/n_e$ .

231 Following the onset of tunnelling the effective carrier mobility increases expo-  
 232 nentially with respect to carrier concentration. The mobility  $\mu_t$  is eventually  
 233 limited by other scattering processes, for example ionized-impurity scattering.  
 234 A semi-empirical relationship the mobility due to the tunnelling of free carriers  
 235  $\mu_t$  can be expressed according to

$$\mu_t = \frac{\mu_{ii} - \mu_{ig}}{1 + \exp[-\frac{1}{\alpha}(\Delta_{BM} + E_R - \beta\Phi_B)]} \quad (13)$$

236 where the factor  $\alpha$  accounts for the sharpness of the onset in tunnelling and  
 237 is likely to be related to the depletion width of the grain boundary. A second  
 238 empirical factor,  $\beta$  takes into account of any extra functional dependence of  $\Phi_B$   
 239 on  $n_t$  which is likely vary with respect to  $n_e$ . The effective mobility may therefore  
 240 be expressed as the sum of the inter-grain and tunnel mobilities according to

$$\mu_{eff} = \mu_{ig} + \mu_t \quad (14)$$

241 Figure 5 shows corresponding the fit of this extended model to the data in the  
 242 region of composition  $x < 0.65\%$ . An extracted value of  $n_t = 1.79 \times 10^{14} \text{ cm}^{-3}$  is  
 243 over two orders of magnitude greater than that reported for reactively sputtered,  
 244 undoped ZnO films [27] and an order of magnitude greater than that for Al  
 245 doped ZnO films [28]. This is reflected in the relatively low optimum mobility  
 246 values of  $\sim 16 \text{ cm}^2\text{V}^{-1}\text{s}^{-1}$  which is typically half that of Al doped ZnO films.  
 247 The reduction of the level trap densities at the grain boundaries is therefore key  
 248 to the improvement of carrier mobility in Si doped ZnO films. This is likely to  
 249 be achieved through further investigations of the effect of growth parameters,  
 250 i.e. substrate temperature and sputter pressure. Based on the model used in  
 251 this work, a reduction of  $n_t$  by  $\sim 20\%$  could yield a doubling of the mobility.

252 The green data points in figure 5 show the  $n_e$  versus  $\mu_e$  behaviour for  $>$   
 253  $0.65\%$  wt.  $\text{SiO}_2$  compositions. The mobility now tends towards a minimum  
 254 value at a higher carrier concentration of  $\sim 3 \text{ cm}^2\text{V}^{-1}\text{s}^{-1}$ . This is indicative of  
 255 an increased trap density, the result of an excess of Si at the grain boundaries  
 256 or perhaps the formation of  $\text{Si}_2\text{O}_3$  phases.

## 5. Conclusions

A consideration of the non-parabolicity of the conduction band for Si doped ZnO has yielded estimates for the values of the band minimum effective mass,  $m_{e0} = 0.35m_0$ , and the non-parabolicity factor,  $C = 0.3 \text{ eV}^{-1}$ . The non-parabolicity contributes to a reduction in the expected Burstein-Moss shift of the optical band-gap at carrier concentrations beyond  $10^{20} \text{ cm}^{-3}$ . Further reductions in the band-gap arises from the renormalization effects which are dominated by electron-electron and electron-ion interactions. For Si doped films the component of the magnitude of these effects are significantly greater than that reported for sputtered Al doped ZnO films.

The combinatorial methodology employed within this work allows the relationship between composition and the electrical behaviour to be determined with excellent accuracy, with a continuous distributions between  $n_e$ ,  $\mu_e$ ,  $\rho$  and % wt.  $\text{SiO}_2$  being determined. Furthermore, the extraction of all data from a single sample ensures that a high level of consistency between each data point is achieved compared with measurements taken over a series of separately deposited samples. Maximum values of  $4.5 \times 10^{20} \text{ cm}^{-3}$  and  $16 \text{ cm}^2\text{V}^{-1}\text{s}^{-1}$  were achieved for the carrier concentration and mobility respectively, at an optimal composition of  $x = 0.65\%$  wt.  $\text{SiO}_2$ , and this corresponding to a minimum resistivity of  $8.7 \text{ }\Omega\text{.cm}$ .

The model of grain boundary scattering proposed by *Seto* [26] has been extended to include the effects of tunneling through grain boundaries. The model generates a good agreement for the observed  $\mu_e$  versus  $n_e$  behaviour at compositions up to the optimum value of  $x$ . The model highlights a potential route to improving carrier mobility, i.e. by reducing the density of trap states that exist at the grain boundaries.

Above the optimum composition a different dependence is observed to that below it. This is thought to be due to the increased density of trap states associated with the incorporation of excess Si into the films.

[1] T. Minami, *Semicond. Sci. Technol.* 20 (2005) S35.

- 287 [2] J. Hu, R. Gordon, *Solar Cells* 30 (1991) 437–450.
- 288 [3] R. E. Treharne, K. Durose, *Thin Solid Films* 519 (2010) 7579–7582.
- 289 [4] J. Rousset, E. Saucedo, D. Lincot, *Chem. Mater.* 21 (2009) 534–540.
- 290 [5] P. R. Chalker, P. A. MARshall, S. Romani, J. Roberts, W. Joseph, S. J. C.  
291 Irvine, D. Lamb, A. Clayton, J. Andrew, P. A. Williams, *J. Vac. Sci. Tech-  
292 nol. A* 31 (2012) 01A120–01A120.
- 293 [6] S. Y. Myong, S. J. Baik, C. H. Lee, W. Y. Cho, K. S. Lim, *Jpn. J. App.  
294 Phys.* 36 (1997) L1078.
- 295 [7] S.-M. Park, T. Ikegami, K. Ebihara, S.-M. Shin, Paik-Kyun Park,  
296 T. Ikegami, K. Ebihara, P.-K. Shin, *App. Surf. Sci.* 253 (2006) 1522–1527.
- 297 [8] T. Minami, T. Miyata, Y. Ohtani, Y. Mochizuki, *Jpn. J. App. Phys.* 45  
298 (2006) L409–L412.
- 299 [9] K. Ellmer, *J. Phys. D: Appl. Phys* 34 (2001) 3097–3108.
- 300 [10] R. E. Treharne, K. Hutchings, D. A. Lamb, S. J. C. Irvine, D. Lane,  
301 K. Durose, *J. Phys. D: Appl. Phys* 45 (2012) 335102.
- 302 [11] D. Mergel, Z. Qiao, *J. Phys. D: Appl. Phys* 35 (2002) 794.
- 303 [12] N. Ashkenov, B. N. Mbenkum, C. Bundesmann, V. Riede, M. Lorenz,  
304 D. Spemann, E. M. Kaidashev, A. Kasic, M. Schubert, M. Grundmann, J.  
305 *Appl. Phys.* 93 (2003) 126–133.
- 306 [13] J. A. Nelder, R. Mead, *The Computer Journal* 7 (1965) 308–313.
- 307 [14] H. A. Macleod, *Thin-Film Optical Filters*, Adam Hilger Ltd, 1986.
- 308 [15] Urbach (????).
- 309 [16] C. Herzinger, B. Johs, W. McGahan, J. Woollam, W. Paulson, *Journal of  
310 Applied Physics* 83 (1998) 3323–3336.

- 311 [17] V. Srikant, D. R. Clarke, J. Appl. Phys. 83 (1998) 5447–5451.
- 312 [18] T. Pisarkiewicz, A. Kolodziej, Phys. Stat. Sol. B 158 (1990) K5–K8.
- 313 [19] R. J. Mendelsberg, Photoluminescence of ZnO grown by eclipse pulsed laser  
314 deposition, Ph.D. thesis, University of Canterbury, New Zealand, 2009.
- 315 [20] F. Ruske, A. Pflug, V. Sittinger, B. Szyszka, D. Greiner, B. Rech (????).  
316 Article in press - Thin Solid Films.
- 317 [21] E. Burstein, Physical Review 93 (1954) 632–633.
- 318 [22] T. S. Moss, Proceedings of the Physical Society. Section B 67 (1954) 775.
- 319 [23] J. Lu, S. Fujita, T. Kawaharamura, H. Nishinaka, Y. Kamada, T. Ohshima,  
320 Z. Ye, Y. Zeng, Y. Zhang, L. Zhu, et al., J. Appl. Phys. 101 (2007) 083705–  
321 083705.
- 322 [24] S. Jain, J. McGregor, D. Roulston, Journal of applied physics 68 (1990)  
323 3747–3749.
- 324 [25] S. C. Jain, D. J. Roulston, Sol. State. Elec. 34 (1991) 453–465.
- 325 [26] J. Y. W. Seto, J. Appl. Phys. 46 (1975) 5247–5254.
- 326 [27] P. F. Carcia, R. S. McLean, M. H. Reilly, G. Nunes, App. Phys. Lett. 82  
327 (2003) 1117–1119.
- 328 [28] M. Kon, P. Song, Y. Shigesato, P. Frach, S. Ohno, K. Suzuki, Jpn. J. App.  
329 Phys. 42 (2003) 263–269.
- 330 [29] B. Johs, J. A. Woollam, C. M. Herzinger, J. Hilfiker, R. Synowicki, C. L.  
331 Bungay, Crit. Rev. Opt. Sci. CR72 (1999) 29–58.
- 332 [30] R. J. Mendelsberg, Y. Zhu, A. Anders, J. Phys. D: Appl. Phys 45 (2012)  
333 425302.

Parameter 1	Extracted Value	Copmparison [23]
$A (\times 10^{-8} \text{ eV.cm})$	$2.1 \pm 0.8$	0.69
$B (\times 10^{-7} \text{ eV.cm}^{3/2})$	$3.0 \pm 2.6$	1.6
$C (\times 10^{-7} \text{ eV.cm}^{3/4})$	$8.7 \pm 1.5$	7.76
$E_{G0} (\text{eV})$	$3.41 \pm 0.01$	-

Table 1: Parameter values extracted from the downhill-simplex fit of equation 7 to the data.  $E_G$  values were extracted from fits to ellipsometry spectra taken in the vicinity of the band gap and  $n_e$  values were determined by Hall measurements. The coefficients A, B and C correspond to the amplitudes of the separate  $n_e^{1/3}$ ,  $n_e^{1/4}$ ,  $n_e^{1/2}$  dependencies respectively of the renormalisation effects.

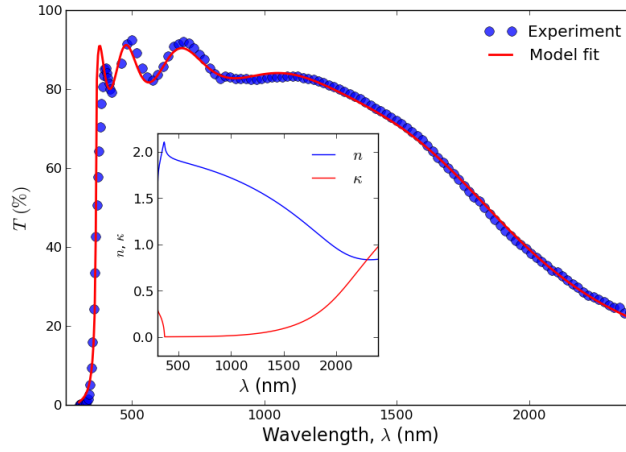


Figure 1: Example of a typical transmittance curve taken from a single point on the combinatorial ZnO:Si sample. The line (—) shows the corresponding fit generated by the dielectric model [10]. An excellent fit is achieved at wavelengths in the vicinity of plasma edge, i.e.  $\lambda > 1000 \text{ nm}$ . The band to band transition component of the model is insufficient to accurately describe the behaviour in the vicinity of the material's direct band gap. In this instance, values of  $d = 518 \pm 10 \text{ nm}$ ,  $\varepsilon_{\infty}\omega_p = 0.97 \pm 0.02 \text{ eV}$  and  $E_G = 3.38 \pm 0.04 \text{ eV}$  were extracted from the fitting procedure. The inset also shows the dispersion relationships for  $n$  and  $\kappa$  extracted by the model.

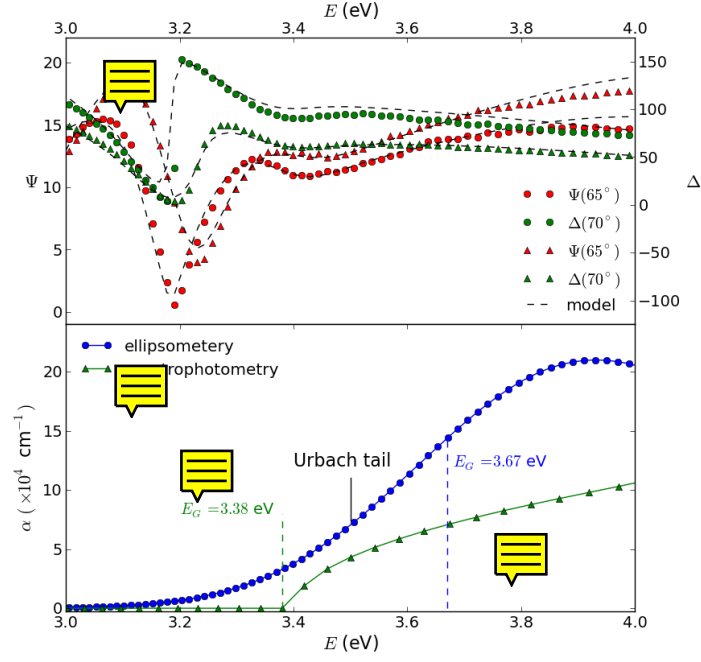


Figure 2: a) Ellipsometric spectra ( $\Psi$  and  $\Delta$ ), measured at separate angles of  $65^\circ$  and  $70^\circ$ , were fitted over the range 3 eV (413 nm) to 4 eV (309 nm) using a single PSEMI-MO oscillator [16, 29], b) The corresponding absorption coefficient extracted from the ellipsometric data compared with that extracted from the spectrophotometric data (1). A difference in the direct band gap of  $\sim 0.3$  eV is determined between the two optical extraction methods. The ellipsometric model is deemed to be more reliable due to its ability to account for the Urbach tail that arises from a distribution of impurity states located just below the bottom of the conduction band.

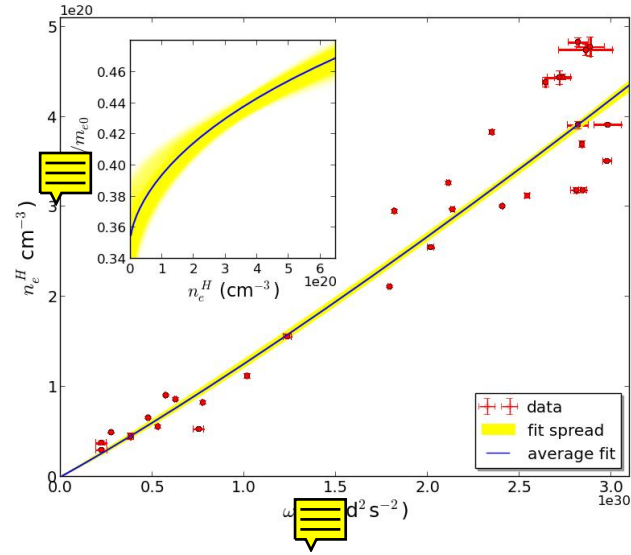


Figure 3: Carrier concentration,  $n_e^H$ , determined via Hall effect measurements versus values of  $(\epsilon_0 \text{ [eV]})$  extracted from the dielectric modeling of transmittance data. A Monte-Carlo style fitting procedure [19, 30] indicates that the relationship between the axes is non-linear, as expected for a material with a non-parabolic conduction band. The spread in uncertainty associated with the fitting procedure is shown by the yellow line. The corresponding relationship between the carrier effective mass,  $m_e$  and the carrier concentration is shown in the inset. Values of  $m_{e0} = 0.35 \pm 0.02 m_0$  and  $C = 0.30 \pm 0.01 \text{ eV}^{-1}$  were extracted from the analysis.



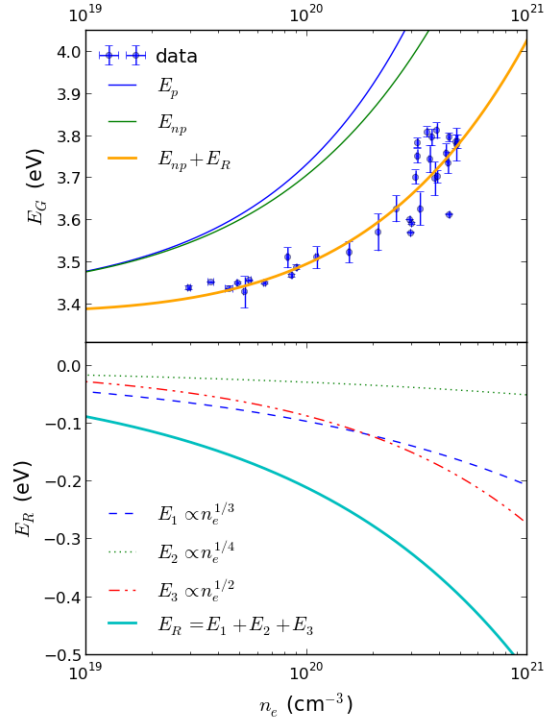


Figure 4: a) Ellipsometry extracted band gap values,  $E_G$ , plotted with respect to the carrier concentration determined by Hall measurements. The Burstein-Moss relation ( $E_p$ ), even once non-parabolicity is accounted for ( $E_{np}$ ), is insufficient to predict the observed relationship - band gap values being significantly lower than expected. The incorporation of renormalization effects permits the data to be fitted. b) The total renormalization energy and each of its subcomponents are shown. The amplitude of these components is calculated empirically via a Monte-Carlo fitting procedure using the model proposed by [24].

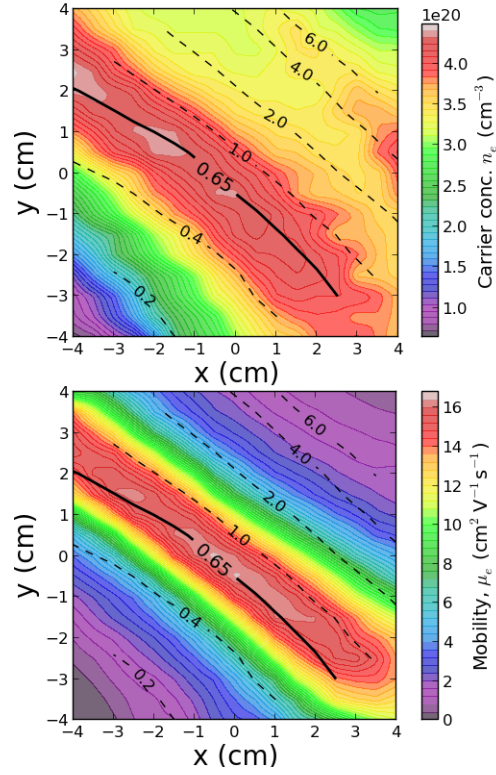


Figure 5: 3D contour plots of the carrier concentration and mobility over the combinatorial sample. All values were extracted using the automated spectrophotometric mapping procedure. The ( - - ) contour lines show an overlay of the % wt.  $\text{SiO}_2$  composition.

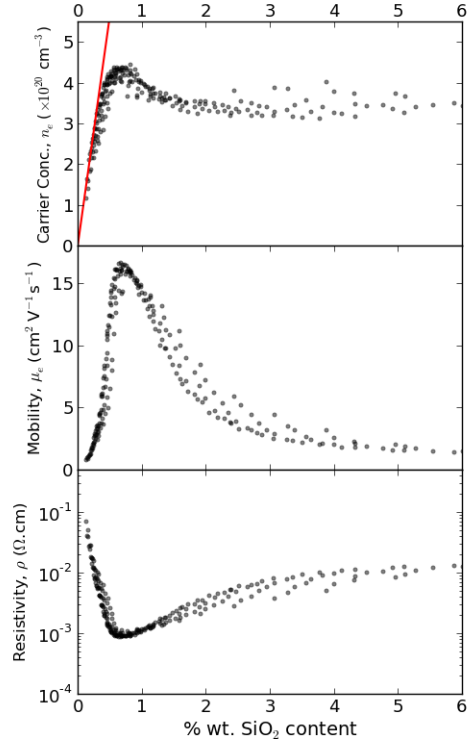


Figure 6: Distributions of carrier concentration, mobility and resistivity with respect to % wt.  $\text{SiO}_2$  content. The maximum values for  $n_e$  ( $4.4 \times 10^{20} \text{ cm}^{-3}$ ) and  $\mu_e$  ( $16.5 \text{ cm}^2 \text{V}^{-1} \text{s}^{-1}$ ) coincide with a composition of 0.65% wt  $\text{SiO}_2$ . The solid straight line (—) in the top plot shows the maximum theoretical carrier concentration achievable if every Si atom incorporated onto a zinc site contributes two free electrons to the system.

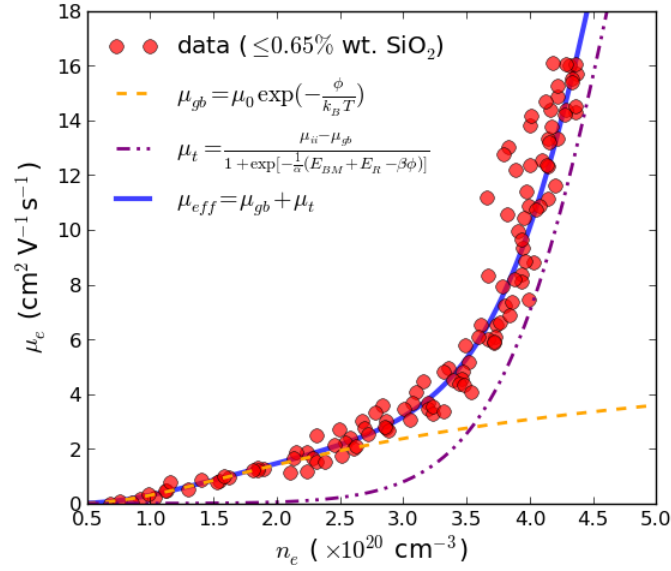


Figure 7: Relationship between  $n_e$  and  $\mu_e$  values extracted from the automated spectrophotometric mapping procedure. All data points have compositions below and up to the optimum value of 0.65% wt.  $\text{SiO}_2$ . The line (—) shows the fit achieved to the data using equations 10-14. The parameter values  $n_t = 1.7 \times 10^{14} \text{ cm}^2$ ,  $L = 40 \text{ nm}$ ,  $\alpha = 25 \text{ eV}$  and  $\beta = 0.54$  were extracted from a downhill-simplex fitting procedure [13]. An estimated value of  $\mu_{ii} = 40 \text{ cm}^2 \text{V}^{-1} \text{s}^{-1}$  was chosen for the fitting but the extracted values were shown to be relatively independent of  $\mu_{ii}$  in the range  $20 - 100 \text{ cm}^2 \text{V}^{-1} \text{s}^{-1}$ .